Elastic wave mode decoupling for full waveform inversion

T.F. Wang, J.B. Cheng and C.L. Wang, Tongji University

January 14, 2015

Introduction

In 1980's, Tarantola (1986) and Mora (1987) have given the theoreotical frameworks for elastic full waveform inversion (EFWI). Recently, people begin to pay more attention to EFWI and its application to real data (Sears et al., 2010; Mora et al., 2014), and even elastic anisotropy becomes a hotspot for FWI (Kamath and Tsvankin, 2013; Oh and Min, 2014; Kim et al., 2014). Different with acoustic FWI, elastic FWI will introduce more parameters and the trade-off between parameters will increase the ill-posedness of the inverse problem. To investigate the trade-off between elastic parameters, diffraction patterns of different parameterizations have been studied for isotropic and VTI media (Wu and Aki, 1985; Tarantola, 1986; Kim et al., 2014; Kamath and Tsvankin, 2014).

To mitigate the ill-posedness of FWI, multi-parameter inversion always need multistage strategies, in which one should successively operate on different parameter classes or differen subsets of seismic data, e.g., Tarantola (1986); Brossier et al. (2009); Raknes and Arntsen (2014). Sears et al. (2008) introduced a successful hierachical strategy using different subsets obtained by temporal windowing for OBC data. In this paper, we discuss another powerful tool, namely elastic wave mode decoupling, to obtain subsets of data for EFWI. For simplisity, we focus on constant-density isotropic media. We first give the gradients of the misfit function built by crossrelating the incident wavefield emitted from the source and the back-propagated residual wavefields. Then we apply mode decoupling to gradient calculations to reduce the trade-off between the elastic parameters, λ and μ. Finally, we apply our method with the new gradients to synthetic transmission data.

Parameter trade-off in EFWI

The full waveform inversion is driven by minimising the misfit function C, between observed data and modelled data in a least-square sense:

$$C = \sum_S \int_0^T dt \sum_R \|d_{mod} - d_{obs}\|^2, \tag{1}$$

where d_{mod} are the synthetic data using the estimated model and d_{obs} are the observed data, with residual energy summation over the total recording time for all receivers and shots. For 2D isotropic FWI problem, the gradients of elastic parameters λ and μ are expressed as,

$$\frac{\partial C}{\partial \lambda} = -\int_0^T (\frac{\partial u_x}{\partial x} + \frac{\partial u_z}{\partial z})(\frac{\partial \psi_x}{\partial x} + \frac{\partial \psi_z}{\partial z}), \tag{2}$$

$$\frac{\partial C}{\partial \mu} = -\int_0^T \left[(\frac{\partial u_x}{\partial z} + \frac{\partial u_z}{\partial z})(\frac{\partial \psi_x}{\partial z} + \frac{\partial \psi_z}{\partial x}) + 2\left(\frac{\partial u_x}{\partial x}\frac{\partial \psi_x}{\partial x} + \frac{\partial u_z}{\partial z}\frac{\partial \psi_z}{\partial z}\right)\right], \tag{3}$$

where u and ψ are the forward wavefield emitted from the source and back-propagated residual wavefields, respectively. Diffraction patterns show that there are trade-offs between λ and μ due to the nature of multi-parameter inversion even in the simplest case of isotropy (Wu and Aki, 1985; Tarantola, 1986). As shown in Figure 1, for a point source, $\delta\lambda$ only scatters P wave energy in a PP mode, while $\delta\mu$ scatters both P and S waves in every mode (PP, PS, SP and SS). So we can not distinguish the scattered P-wave energy coming from which parameter perturbation definitely. However, we can confirm that scattered S

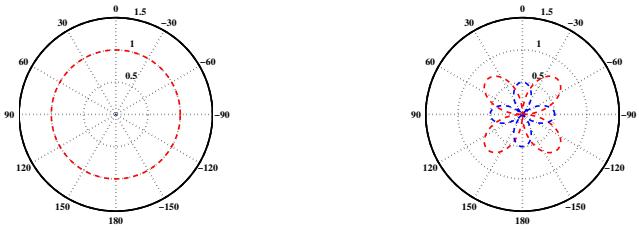

(a) (b)

Figure 1: Normalized diffraction patterns of (a) λ and (b) μ with a point source, the red line represents the scattered P wave energy (PP and SP) while the blue line represents the scattered S wave energy (SS and PS).

wave are only assosiated with μ perturbations. Accordingly, if we use the whole wavefields with both P and S wave to calculate the gradient, then the gradient of μ will be distorted by the P wave scattered from λ if $\delta\lambda$ is stronger than $\delta\mu$. And the gradient of λ will not be distorted if $\delta\mu$ is weak because of the divergence operator in equation 2, which will make sure the gradient is calculated with pure P wave. Taking Account of this, we may alleviate the trade-off between λ and μ through wave mode separation and decomposition.

Wavefield separation and decomposition in gradient calculation

The gradient in equation 2 and 3 are calculated using mixed wavefields, so we can rewrite the equations as:

$$\frac{\partial C}{\partial \lambda} = -\int_0^T (\frac{\partial u_x}{\partial x} + \frac{\partial u_z}{\partial z})(\frac{\partial \psi_x^P + \partial \psi_x^S}{\partial x} + \frac{\partial \psi_z^P + \partial \psi_z^S}{\partial z}) \tag{4}$$

$$\begin{aligned}\frac{\partial C}{\partial \mu} = -\int_0^T [&(\frac{\partial u_x}{\partial z} + \frac{\partial u_z}{\partial x})(\frac{\partial \psi_x^P + \partial \psi_x^S}{\partial z} + \frac{\partial \psi_z^P + \partial \psi_z^S}{\partial x}) \\ &+ 2\left(\frac{\partial u_x}{\partial x}\frac{\partial \psi_x^P + \partial \psi_x^S}{\partial x} + \frac{\partial u_z}{\partial z}\frac{\partial \psi_z^P + \partial \psi_x^S}{\partial z}\right)]\end{aligned} \tag{5}$$

where ψ^P and ψ^S are back-propagated P and S wavefields of data residuals from receivers. To solve equation 4 and 5 requires not only wave mode separation but also wavefield vector decomposition. This can be achieved with (Zhang and McMechan, 2010) :

$$\mathbf{U}^P = \mathbf{K}(\mathbf{K}\cdot\mathbf{U}), \mathbf{U}^S = -\mathbf{K}\times(\mathbf{K}\times\mathbf{U}) \tag{6}$$

where $\mathbf{K} = (k_x, k_y, k_z)$ is the P-wave polarization vector, $\mathbf{U}$ is the vector wavefield, and $\mathbf{U}^P$ and $\mathbf{U}^S$ are separated vector wavefield of P and S wave respectively. As mentioned above, we separate the back-propagated S wave residuals to calculate the gradient of μ in order to guarantee it will not be destorted by the P wave scattered from λ, while the gradient of λ don't need separation because of the intrinsic divergence operator. Thus the modified gradient of μ can be written as:

$$\frac{\partial C}{\partial \mu} = -\int_0^T \left[(\frac{\partial u_x}{\partial z} + \frac{\partial u_z}{\partial x})(\frac{\partial \psi_x^S}{\partial z} + \frac{\partial \psi_z^S}{\partial x}) + 2\left(\frac{\partial u_x}{\partial x}\frac{\partial \psi_x^S}{\partial x} + \frac{\partial u_z}{\partial z}\frac{\partial \psi_z^S}{\partial z}\right)\right] \tag{7}$$

we can see that in equation 7, the calculation makes use of forward propagated P and S wave eneregy and back-propagated S wave. Therefore this gradient will highly sensitive to S wave residuals, which are only generated by μ perturbations. So our method claims enough S wave energy in the data residuals.

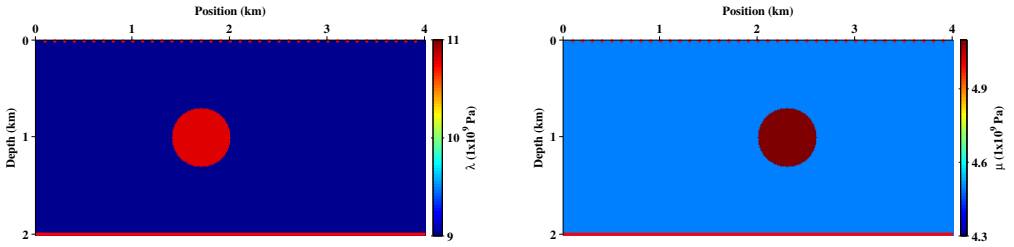

(a) (b)

Figure 2: True elastic parameter of (a) λ and (b) μ, the red spots on top are shot locations and the red line on bottom is receiver array.

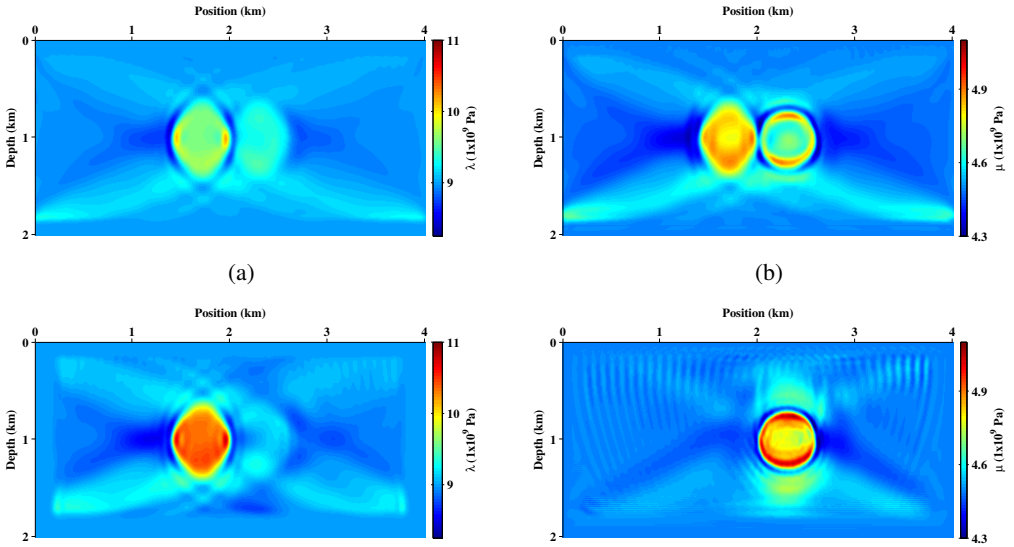

(a) (b)

(c) (d)

Figure 3: Inversion results of conventional and decoupling EFWI with weak S wave. (a) λ and (b) μ are conventional results, (c) λ and (d) μ are results with decoupling.

Examples

To demonstrate our method, we design a simple synthetic model as shown in figure 2, including anomalies in λ and μ located at different position. The initial model for inverstion are the background parameter and $\rho = 2000kg/m^3$. The data are generated by 39 shots with a main frequency of 10 Hz placed in the top and the receivers are placed at the bottom. We test our method on two different sets of data for 20 iterations without hierachical strategy.

First we use the data containing very weak S wave (maximum P S energy ratio 100:1). The inversion results are shown in figure 3. The low frequncy artifacts are due to the lackness of regularization and deficiency of data fold. We can see that the results of conventional EFWI (figure 3(a) and 3(b)) fall into a local minimum, especially for μ. Because the strong P wave energy scattered by $\delta\lambda$ disort the gradient of μ and lead to the failure of estimation of μ. While the EFWI with wave mode decoupling gives a better results (figure 3(c) and 3(d)). But the center of invered μ is not good enough because PS wave will dominate the inverstion due to weak transmitted S wave.Although mode-converted PS-waves are highly sensitive to short-scale features of μ, it is inadequate for μ inversion alone. So the absence of low wavenumber information in the center of μ will cause a leakage into the estimation of λ.

To obtain the intermediate length scale information on μ, we take another test using the data including enough S wave energy (maximum P S energy ratio 10:1). Also, the non-decouple method gives a bad result (figure 4(a) and figure 4(b)) although it is better than (figure 3(a) and figure 3(b)). And our method will acheive a good result (figure 4(c) and figure 4(d)). The intermediate length scale information on μ

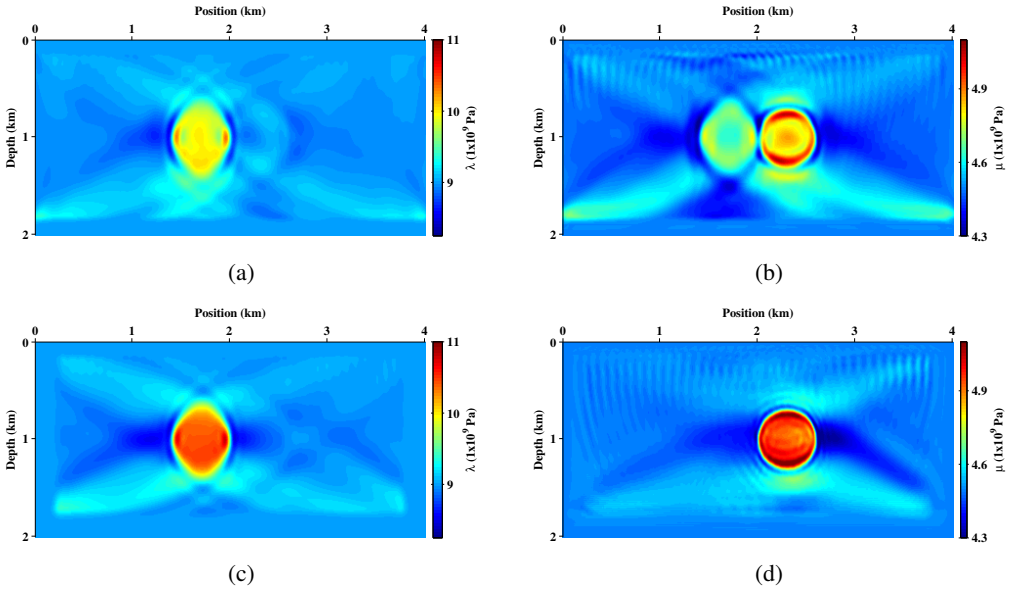

Figure 4: Inversion results of conventional and decoupling EFWI with enough S wave. (a) λ and (b) μ are conventional results, (c) λ and (d) μ are results with decoupling.

can be recovered from P wave AVO response (Sears et al., 2010), or from S-S and PS-S wave data, to avoid the short-scale information from PS-wave data dominating the inversion and falling into a local minimum. Due to the probability of wrong update of μ introduced by P wave AVO response, we suggest the utilization of S-S or PS-S if they are available.

Conclusions

We calculate the gradients of EFWI with wave mode decoupled data to alleviate the trade-off between parameters. Our method claims enough S wave energy in the data residuals. Lots of kinds of S wave energy will satisfy the requirement, including S-S, P-S and even PS-S when there is strong PS conversion occured. The synthetic examples demonstrate that strategy with wave mode decoupling will give better results in simultaneous multi-parameter EFWI.

Acknowledgement

We appreciate the support of Madagascar open-source package freely from: *http://www.reproducibility.org*

REFERENCES

Brossier, R., S. Operto, and J. Virieux, 2009, Seismic imaging of complex onshore structures by 2d elastic frequency-domain full-waveform inversion: Geophysics, **74**, WCC105–WCC118.

Kamath, N., and I. Tsvankin, 2013, Gradient computation for elastic full-waveform inversion in 2d vti media: 83rd Annual International Meeting, SEG, Expanded Abstracts.

———, 2014, Sensitivity analysis for elastic full-waveform inversion in vti media: IWSA expanded abstract, 16.

Kim, W., D. Min, and S. Kim, 2014, A new parameterisation for 2d elastic vti media: 76th EAGE Conference and Exhibition 2014, Expanded Abstracts.

Mora, D., K. Jiao, D. Watts, and D. Sun, 2014, Elastic full-waveform inversion application using multi-component measurements of seismic data collection: Geophysics, **79**, R63–R77.

Mora, P., 1987, Nonlinear two-dimensional elastic inversion of multioffset seismic data: Geophysics, **52**, 1211–1228.

Oh, J., and D. Min, 2014, Multi-parametric fwi using a new parameterisation for elastic vti media: 76th EAGE Conference and Exhibition 2014, Expanded Abstracts.

Raknes, E. B., and B. Arntsen, 2014, Strategies for elastic full waveform inversion: 2014 SEG Annual Meeting.

Sears, T., S. Singh, and P. Barton, 2008, Elastic full waveform inversion of multi-component OBC seismic data: Geophysical Prospecting, **56**, 843–862.

Sears, T. J., P. J. Barton, and S. C. Singh, 2010, Elastic full waveform inversion of multicomponent ocean-bottom cable seismic data: Application to Alba Field, U.K. North Sea: Geophysics, **75**, R109–R119.

Tarantola, A., 1986, A strategy for nonlinear elastic inversion of seismic reflection data: Geophysics, **51**, 1893–1903.

Wu, R., and K. Aki, 1985, Scattering characteristics of elastic waves by an elastic heterogeneity: Geophysics, **50**, 582–595.

Zhang, Q., and G. A. McMechan, 2010, 2D and 3D elastic wavefield vector decomposition in the wavenumber domain for VTI media: Geophysics, **75**, D13–D26.